Nanoscale

ROYAL SOCIETY OF CHEMISTRY

COMMUNICATION

View Article Online
View Journal | View Issue

Check for updates

Cite this: *Nanoscale*, 2023, **15**, 7710

Received 7th December 2022,
Accepted 30th January 2023

DOI: 10.1039/d2nr06840k

rsc.li/nanoscale

Published on 31 januar 2023. Downloaded on 11.7.2024 12:26:06.

Investigating the interfacial properties of halide perovskite/TiO_x heterostructures for versatile photocatalytic reactions under sunlight†

Tae Hyung Kim,[a] Inho Park,[a] Kyeong Ho Lee,[a] Jin-Han Sim,[b] Min-Ho Park,[c] Tae-Hee Han,[b] Ungyu Paik,[a] Jaeyoung Jang,*[a] Ho Bum Park*[a] and Young-Hoon Kim*[a]

Heterostructures of metal halide perovskites and TiO_x are efficient photocatalytic materials owing to the combination of the advantages of each compound, specifically the high absorption coefficients and long charge-carrier lifetimes of perovskites, and efficient photocatalytic activity of TiO_x. However, chemical reduction of CO_2 using PNC/TiO_x heterostructures without organic solvents has not been reported yet. Here, we report the first solvent-free reduction of CO_2 using amorphous TiO_x with embedded colloidal perovskite nanocrystals (PNCs). The combination was obtained by carrying out hydrolysis of titanium butoxide (TBOT) on the PNC surface without high-temperature calcination. We proposed a mechanism involving photoexcited electrons being transferred from PNCs to TBOT, enabling photocatalytic reactions using TiO_x under visible-light excitation. We demonstrated efficient visible-light-driven photocatalytic reactions at PNC/TiO_x interfaces, specifically with a CO production rate of 30.43 μmol g^{-1} h^{-1} and accelerated degradation of organic pollutants under natural sunlight. Our work has provided a simple path toward both efficient CO_2 reduction and photocatalytic degradation of organic dyes.

Introduction

As human civilization went through the industrial revolution and the population has increased, our world faces serious global crises, especially global warming[1] and water pollution, both of which threaten the environment and human civilization. Various strategies for decreasing CO_2 emissions and water pollutants have been attempted: biological,[2] electrochemical,[3] photochemical[4] and photoelectrochemical[5] conversion techniques have been tested for converting CO_2 to valuable chemicals and fuels; and biodegradation,[6] electrochemical oxidation[7] and photocatalytic reduction[8] have been applied to eliminate dye contaminations. Of these strategies, use of photocatalysts is considered the most promising one for decreasing both atmospheric CO_2 gas and organic pollutants because photocatalysts have wide applicability and can degrade organic materials to harmless products such as H_2O and H_2. This ability can be exploited to reduce CO_2 emission and degrade water pollutants. The process can be also powered by sunlight, which is free and essentially infinite. Photochemical reactions to decrease the amounts of CO_2 or water pollutants have been achieved using various materials such as metal oxides (*e.g.*, TiO_2, Cu_2O, WO_3, Bi_2WO_6, Zn_2GeO_4, $ZnGa_2O_4$, oxide perovskites),[9–11] metal–organic frameworks,[12] nitrides (*e.g.*, C_3N_4, GaN, $(Zn_{1+x}Ge)(N_2O_x)$),[13] sulfides (*e.g.*, CdS, ZnS and Cu_2ZnSnS_4),[14] and phosphides (*e.g.*, InP, GaP).[15] However, these materials have wide bandgaps (for instance, >3.2 eV for TiO_2,[16] and >3.25 eV for WO_3[17]), so they initiate catalytic reactions only under ultraviolet (UV) light (wavelength λ < 400 nm). However, only less than 5% of sunlight has photons in these wavelengths, so photocatalytic reactions in conventional photocatalytic materials require an additional UV source. Also, in these conventional materials, recombination of charge carriers is rapid, so the photocatalytic reaction efficiency is relatively poor. Therefore, efficient chemical reduction of CO_2 and degradation of organic pollutants under sunlight require new materials that use wavelengths >400 nm, have high absorption coefficients, and show slow recombination of charge carriers and efficient photocatalytic reaction capabilities.

To achieve these goals, heterostructures in which an "absorber" traps light and transfers excited electrons to a "photocatalyst" have been tested. Halide perovskites have been regarded as promising light absorbers due to their high absorption coefficients, long carrier diffusion paths, long

[a]*Department of Energy Engineering, Hanyang University, 222 Wangsimni-ro, Seongdong-gu, Seoul 04763, Republic of Korea. E-mail: jyjang15@hanyang.ac.kr, badtzhb@hanyang.ac.kr, younghoonkim@hanyang.ac.kr*
[b]*Division of Materials Science and Engineering, 222 Wangsimni-ro, Seongdong-gu, Seoul 04763, Republic of Korea*
[c]*Department of Materials Science and Engineering, Department of Green Chemistry and Materials Engineering, Soongsil University, 369 Sangdo-Ro, Dongjak-Gu, Seoul 06978, Republic of Korea*

† Electronic supplementary information (ESI) available. See DOI: https://doi.org/10.1039/d2nr06840k

This journal is © The Royal Society of Chemistry 2023

Published on 31 januar 2023. Downloaded on 11.7.2024 12:26:06.

charge carrier lifetimes and tunable bandgaps.[18,19] Amorphous TiO_2 (TiO_x) or crystalline TiO_2 are efficient photocatalysts due to their electrical conductivity, decent photocatalytic activity and excellent chemical stability levels.[20]

Halide perovskite nanocrystals (PNCs) embedded in TiO_x matrices[21] or in TiO_2 nanofibers[22] have been developed to facilitate chemical reduction of CO_2 by virtue of the photoinduced excitation of charges in the PNCs and transfer and extraction of these excited charges to TiO_x. These reactions are generally carried out with an external power supply (under Xe-lamp irradiation, which covers the ultraviolet-visible light range (100 nm < $\lambda \leq$ 800 nm)), with the CO_2 reduction rates measured in the presence of organic solvents (ethyl acetate,[21] acetonitrile[22]). Natural sunlight, which is an essentially infinite resource, can be utilized to realize the photocatalytic reactions, which would decrease both CO_2 emissions and generation of water pollutants without use of an additional external power consumption. To the best of our knowledge, the chemical reduction of CO_2 using PNC/TiO_x (or TiO_2) heterostructures under sunlight illumination has not been reported. Moreover, perovskite-photocatalyzed reduction of CO_2 is often overestimated in CO_2 reduction experiments that are conducted in the presence of organic solvents because the organic solvents can be transformed (at a rate of, for example, ~1 mmol g^{-1} h^{-1}) into reduced products such as CO and CH_4.[23] So far, CO_2 reduction using PNC/TiO_x heterostructures without organic solvents has not been reported.

Here we developed a reduction of CO_2 not involving the use of an organic solvent by using PNC/TiO_x heterostructures in which the PNCs absorbed visible sunlight and boosted the photocatalytic reactions at the TiO_x component. TiO_x formed on the surfaces of $CsPbBr_3$ PNCs as a result of hydrolysis of titanium butoxide (TBOT) without high-temperature calcination. We proposed a mechanism involving transfer of photoexcited electrons to TBOT, allowing for the first solvent-free CO_2 reduction based on PNC/TiO_x heterostructures. PNC/TiO_x heterostructures decreased CO_2 concentration at a rate of 30.43 μmol g^{-1} h^{-1} under outdoor sunlight without use of any other external energy. Moreover, we demonstrated more efficient degradation of organic dye under visible white light (λ = 400 nm–780 nm), green light (λ = 500–520 nm) and outdoor sunlight by PNC/TiO_x heterostructures than by pure PNCs and TiO_x.

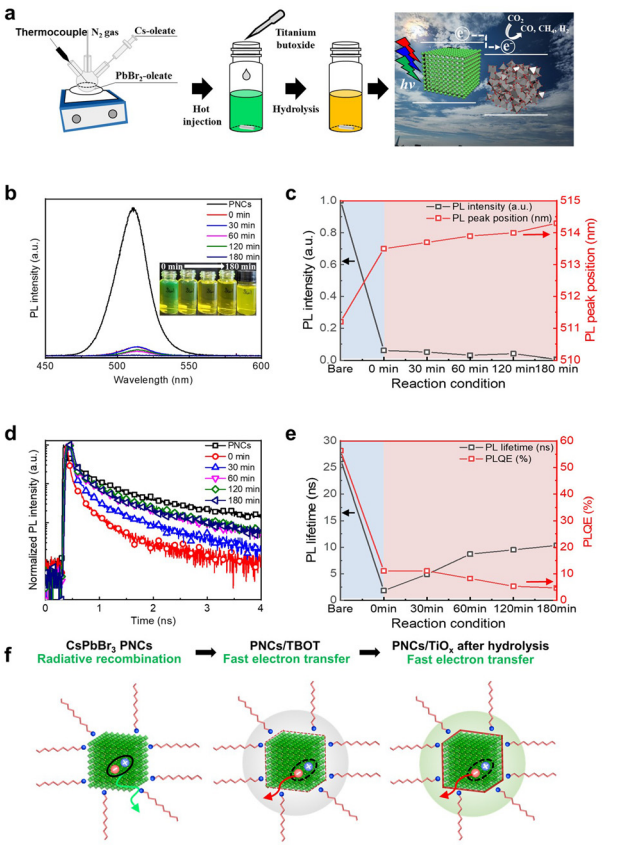

Fig. 1 (a) Schematic illustrations of the introduction of TBOT into $CsPbBr_3$ PNCs (left), subsequent hydrolysis of TBOT (middle), and photocatalytic reactions of $CsPbBr_3/TiO_x$ heterostructures under sunlight (right). (b) PL spectrum (inset: optical images of solutions), (c) PL intensity and PL peak wavelength as a function of reaction time, (d) time-resolved PL spectra, (e) PL lifetime and PLQE and (f) schematic illustrations of charge carrier behaviors for formation of $CsPbBr_3/TiO_x$ heterostructures under continuous hydrolysis.

Results and discussion

Synthesis of PNC/TiO_x heterostructures

PNC/TiO_x heterostructures were synthesized by introducing and then hydrolyzing TBOT ($O–Ti(OC_4H_9)_4$) on the surface of pre-synthesized $CsPbBr_3$ PNCs (Fig. 1a). Before synthesis of the heterostructures, the PNCs were cubic with an average size of 9.4 nm, and showed a peak at 511.1 nm in the PL spectrum, with an FWHM of 20 nm (Fig. S1a and b†). After injection of TBOT, the PNC solutions showed a significant decrease in PL intensity with a sudden redshift of the peak in the PL spectrum from 511.1 nm to 514.3 nm, attributed to TBOT having adhered to the surfaces of the PNCs and inducing severe exciton dissociation in them (Fig. 1b and c). As the TBOT was hydrolyzed in air with 40% humidity, composite solutions showed a gradual change of color from bright green to turbid yellow (Fig. 1b, inset), and a gradual decrease of PL intensity with a redshift of the PL signal (Fig. 1c, and S2†).

Photophysical properties

To quantify the charge carrier dynamics in the composites, we measured PL lifetimes, and did so by conducting time-correlated single-photon counting (TCSPC) with excitation laser irradiation (wavelength = 405 nm) of the composite solutions. After injection of TBOT into $CsPbBr_3$ PNCs, the heterostructures showed dramatically decreased τ_{ave} (from τ_{ave} of 26.51 ns for $CsPbBr_3$ PNCs to τ_{ave} of 1.8 ns for $CsPbBr_3$/TBOT composites) due to exciton quenching and electron transfer by TBOT on the PNC surfaces (Fig. 1d, e, and Table S1†). This result corresponded well to the observed sudden decrease in PL intensity (Fig. 1b and c). After the initial rapid decrease in

Published on 31 janiar 2023. Downloaded on 11.7.2024 12:26:06.

PL lifetime upon addition of TBOT, the composite solutions showed gradually increasing τ_{ave} (τ_{ave} = 10.33 ns, heterostructures with 180 minutes of reaction). These increases in the PL lifetime were opposite the decrease in the PL intensity (Fig. 1c, d, and S2†). We attributed the increase in PL lifetime upon hydrolysis of TBOT to the aggregation of nanoparticles (Fig. S3–6†).

Using measured average PL lifetimes, we investigated the rate of electron transfer k_{ET} from PNCs to TBOT. The k_{ET} parameter was derived using the equation[24]

$$k_{ET} = \frac{1}{\tau_{CsPbBr_3/TBOT}} - \frac{1}{\tau_{CsPbBr_3}} \quad (1)$$

where $\tau_{CsPbBr_3/TBOT}$ and τ_{CsPbBr_3} are the PL lifetimes of the $CsPbBr_3$/TBOT composites and $CsPbBr_3$ PNC, respectively. And k_{ET} of $CsPbBr_3$/TBOT was calculated to be 5.18×10^8, a value 5 times that of the previously reported $CsPbBr_3/TiO_2$ ($k_{ET} = 9.7 \times 10^7$ s^{-1}),[24] indicative of efficient charge transfer at the $CsPbBr_3$/TBOT interface.

Chemical and structural properties

To study the chemical properties of the heterostructure surfaces upon hydrolysis of TBOT, we performed FTIR spectroscopy experiments (Fig. S7a and b†). When TBOT was introduced to the PNC solutions, increases were observed in the intensities of the C–H signals of O–Ti$(OC_4H_9)_4$ at 3430 cm^{-1}, the COO^- and CH_3 signals at 1468–1380 cm^{-1}, the C–H stretching signals at 2923–2854 cm^{-1} (Fig. S7a†) and the Ti–O–C bond signals at 1125–1035 cm^{-1} (Fig. S7b†). As the hydrolysis proceeded, the intensities of these signals decreased linearly; this trend confirmed that TBOT became converted to TiO_x as suggested in the PL and time-resolved PL spectra analysis. When the hydrolysis reaction had finished (180 minutes after initiation of hydrolysis when the PL lifetime, intensity and spectrum stopped changing), heterostructures were collected by performing sequential centrifugation and dried by performing evaporation of residual solvent in vacuum.

Then we determined the crystal structure of $CsPbBr_3/TiO_x$ heterostructures by conducting X-ray diffraction (XRD) spectroscopy (Fig. 2a). The heterostructures yielded clear XRD peaks at 15.1°, 21.1°, 29.8°, 29.9°, 34.7°, 36.9° and 44.6°, which corresponded to (100), (110), (004), (200), (210), (211) and (220) crystal planes, respectively; these observations were consistent with peaks of $CsPbBr_3$ PNCs. Amorphous TiO_x without PNCs did not show any clear XRD peaks. High-resolution TEM showed PNCs embedded in the TiO_x matrix with clear lattice constants of 3.0 and 4.1 Å, which corresponded to, respectively, (002) and (110) planes in the $CsPbBr_3$ PNCs (Fig. S8†). To study the chemical formation and electrical interaction at the interfaces in the heterostructures, we collected X-ray photoelectron spectroscopy (XPS) data from control TiO_x, PNCs and the heterostructures (Fig. 2b–d, and S9†). The heterostructures showed XPS peaks assigned to Br (~68.0 eV), Pb (~137.9 and 143.0 eV) and Ti (~464.2 eV, 458.2 eV), which indicated the presence of both $CsPbBr_3$ and TiO_x.

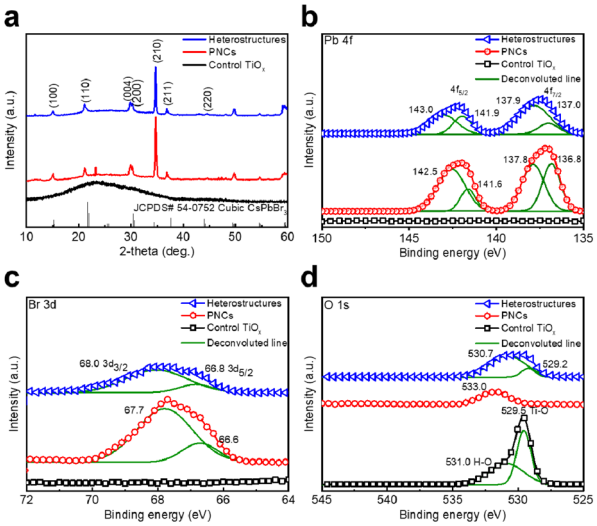

Fig. 2 (a) XRD patterns and (b) Pb 4f, (c) Br 3d and (d) O 1s regions of the XPS spectra of the $CsPbBr_3/TiO_x$ heterostructures, PNCs and control TiO_x.

Signals of Pb and Br from $CsPbBr_3$ in the heterostructures were blue-shifted toward higher binding energy compared to those in PNCs (from ~142.5 eV for $4f_{5/2}$, ~137.8 eV for $4f_{7/2}$, ~67.7 eV for $3d_{3/2}$, ~66.6 eV for $3d_{5/2}$ in PNCs to ~143.0 eV for $4f_{5/2}$, ~137.9 eV for $4f_{7/2}$, ~68.0 eV for $3d_{3/2}$, ~66.8 eV for $3d_{5/2}$ in heterostructures). These XPS peak shifts indicated that electron transfers from $CsPbBr_3$ to TiO_x occurred at the interface, in turn attributed to a shallower conduction band minimum (CBM) of $CsPbBr_3$ (~−3.9 eV)[25] than of TiO_x (~−4.00 eV).[26] This transfer focused the electrons towards TiO_x and boosted the photocatalytic activity of TiO_x.

Photocatalytic reactions

To evaluate the photocatalytic activities of the heterostructures, we conducted photochemical CO_2 conversion analysis of control TiO_x, PNCs and the heterostructures (results summarized in Table S2†). To prevent side reactions and enable correct measurement of the CO_2 conversion efficiencies of our samples, the light intensity was measured during the reaction (Fig. S10 and Table S3†) and the experiments were performed in a gas–solid reaction system without any sacrificial reagents or organic solvents.[23] First, an external light source was tested for practical analysis. Under visible white light irradiation ($400 \leq \lambda \leq 780$ nm, Fig. S10†), $CsPbBr_3/TiO_x$ heterostructures showed a CO production rate of 12.77 μmol g^{-1} h^{-1} and photoelectron consumption rate of 25.54 μmol g^{-1} h^{-1} (Fig. 3a and b). The CO_2 was reduced to CO by consuming two electrons, and no other gasses such as H_2 were detected. PNCs showed a CO production rate of 7.1 μmol g^{-1} h^{-1}, a value lower than that of the heterostructures, and control TiO_x did not show any CO production, attributed to the inability of TiO_x with its wide bandgap (~4 eV) to absorb visible light ($400 \leq \lambda \leq 780$ nm). Furthermore, control TiO_x, PNCs and $CsPbBr_3/TiO_x$

This journal is © The Royal Society of Chemistry 2023

Published on 31 januar 2023. Downloaded on 11.7.2024 12:26:06.

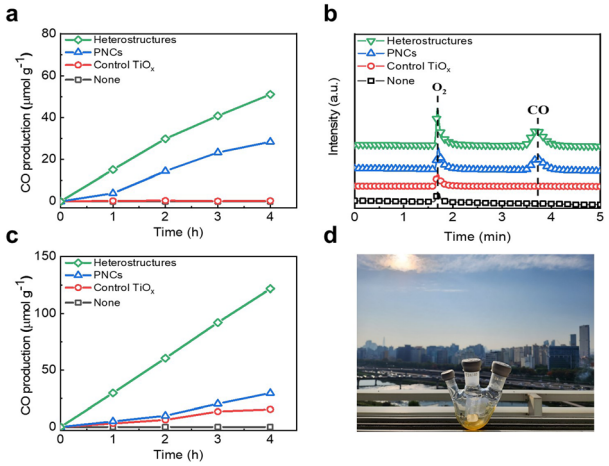

Fig. 3 (a) CO-production rates and (b) GC chromatograms of a sample without any photocatalytic materials ("none"), control TiO_x, PNCs and heterostructures in white-light illumination, (c) CO-production rates and (d) photograph of CO_2 reduction experiment of heterostructures under outdoor natural sunlight.

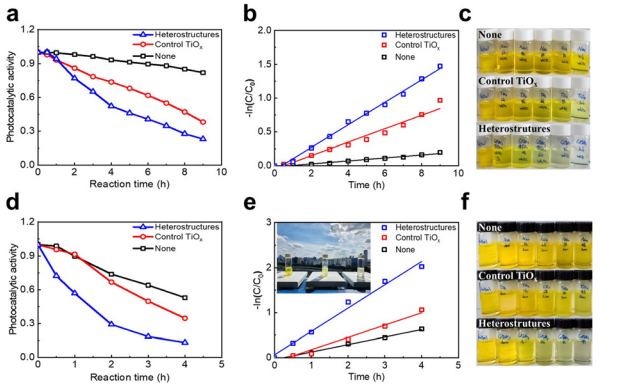

Fig. 4 (a) Photocatalytic degradation activities, (b) kinetic curves, (c) photographs of PPV copolymer degraded without any photocatalytic materials (top), with control TiO_x (middle), and with PNC/TiO_x heterostructures (bottom) under visible white light. (d) Photocatalytic degradation activities, (e) kinetic curves (inset: photograph of experiment) and (f) photographs of PPV copolymer without any photocatalytic materials (top), with control TiO_x (middle), and with PNC/TiO_x heterostructures (bottom) under outdoor natural sunlight.

heterostructures showed CO production rates of 3.87, 7.44 and 30.43 μmol g^{-1} h^{-1}, respectively, under natural sunlight without any additional light source such as an Xe lamp or LED light (Fig. 3c and d). To the best of our knowledge, this was the first reported example of a perovskite/TiO_x-heterostructure-based reduction of CO_2 carried out without using organic solvent.

To further investigate the photocatalytic activities of the heterostructures, we conducted a photocatalytic degradation of orange-light-emitting PPV copolymer (Merck Orange) under white light ($400 \leq \lambda \leq 780$ nm), green light ($450 \leq \lambda \leq 600$ nm) and outdoor natural sunlight. The degradations were monitored by tracking maximum absorbance (Fig. S12 and S13†), observing the solution color with the naked eye, and FTIR spectroscopy (Fig. S14†). The dye degraded much more rapidly in the solution with heterostructures than with control TiO_x and without any catalytic materials: degradation rates of 77.1% with heterostructures, 62% with control TiO_x and 18% without any photocatalytic reactors for 9 hours (h) under white light (Fig. 4a, S12a–c†); 57% for heterostructures, 47.7% for control TiO_x and 8.6% for samples without any photocatalytic reactors for 16 h under green light (Fig. S12d–f, and S15†); and 86.8% with heterostructures, 65.4% with control TiO_x and 47.1% with samples without any photocatalytic reactors for 4 h under outdoor sunlight (Fig. 4d, S12g–i†). We attributed the degradation of organic dyes with pure TiO_x, which cannot absorb visible light, to the charge carriers excited in orange PPV copolymer having been transferred to TiO_x and then inducing the photocatalytic reaction.[27] All of the degradations of organic dye under light irradiation followed a pseudo-first-order decay according to the equation $\ln(C/C_0) = kt$, where C_0 is the initial concentration of organic dye, C is the concentration of organic dye at reaction time t, and k is the absorption coefficient.

Conclusions

We have demonstrated an efficient reduction of CO_2 without organic solvent in PNC systems by forming TiO_x on $CsPbBr_3$ PNC surfaces as a result of hydrolyzing TBOT without high-temperature calcination. Photoexcited electrons in the resulting heterostructures were concluded to be transferred to TBOT and then TiO_x upon conversion of the TBOT to TiO_x, with this transfer slowing the recombination of charge carriers and having achieved in our experiments a solvent-free CO_2 reduction rate of 30.43 μmol g^{-1} h^{-1} under sunlight. To the best of our knowledge, this was the first reported example of PNC/TiO_x-heterostructure-based CO_2 reduction without any organic solvent. We also demonstrated that PNC/TiO_x heterostructures can be used to boost photocatalytic degradation of organic dye under visible white light, green light and outdoor sunlight. This result has suggested the use of halide perovskites as a step towards the development of environmentally benign CO_2 reduction and pollutant reduction.

Note added after first publication

This article replaces the version published on 31st January 2023. Since the first publication, the authors were made aware of a late reviewer's concerns regarding the time-resolved photoluminescence (PL) lifetime data, which the authors and Editorial Office felt it would be best to address. The outcome of this consideration was that the authors re-conducted the experiment and have now attributed the increase in PL lifetime with hydrolysis of TBOT to an artefactual aggregation of nanoparticles during hydrolysis. Minor changes to the text of the main article, including a revision of eqn (1) and removal of eqn (2) in the Results and discussion section, have been made

with the approval of the handling Associate Editor. Changes have also been made to ESI Fig. S3–S6,† most notably the addition of further discussion of the PL lifetimes following Fig. S4.† These changes have been reviewed by the handling Associate Editor and the authors confirm that the main findings of the article have not been significantly altered.

Conflicts of interest

There are no conflicts to declare.

Acknowledgements

This work was supported by the research fund of National Research Foundation of Korea (NRF) grant funded by the Korea government (MSIT) (2022R1A5A1032539, 2022R1C1C1008282) and Industrial Strategic Technology Development Program-Alchemist Project (1415180859, Chiral perovskite LED smart contact lens based hyper vision metaverse) funded by the Ministry of Trade, Industry & Energy (MOTIE, Korea) and Korea Evaluation Institute of Industrial Technology (KEIT, Korea).

Published on 31 januar 2023. Downloaded on 11.7.2024 12:26:06.

References

1 M. Mendez-Galvan, B. Alcantar-Vazquez, G. Diaz, I. A. Ibarra and H. A. Lara-Garcia, *React. Chem. Eng.*, 2021, **6**, 828–838.
2 F. Tassi, S. Venturi, J. Cabassi, O. Vaselli, I. Gelli, D. Cinti and F. Capecchiacci, *Org. Geochem.*, 2015, **86**, 81–93.
3 S. Nitopi, E. Bertheussen, S. B. Scott, X. Liu, A. K. Engstfeld, S. Horch, B. Seger, I. E. L. Stephens, K. Chan, C. Hahn, J. K. Nørskov, T. F. Jaramillo and I. Chorkendorff, *Chem. Rev.*, 2019, **119**, 7610–7672.
4 U. Ulmer, T. Dingle, P. N. Duchesne, R. H. Morris, A. Tavasoli, T. Wood and G. A. Ozin, *Nat. Commun.*, 2019, **10**, 3169–3180.
5 V. Kumaravel, J. Bartlett and S. C. Pillai, *ACS Energy Lett.*, 2020, **5**, 486–519.
6 I. Jambon, S. Thijs, G. Torres-Farradá, F. Rineau, N. Weyens, R. Carleer, P. Samyn and J. Vangronsveld, *Front. Microbiol.*, 2019, **10**, 1892–1904.
7 C. A. Martínez-Huitle and S. Ferro, *Chem. Soc. Rev.*, 2006, **35**, 1324–1340.
8 C. Lu, P. Zhang, S. Jiang, X. Wu, S. Song, M. Zhu, Z. Lou, Z. Li, F. Liu, Y. Liu, Y. Wang and Z. Le, *Appl. Catal., B*, 2017, **200**, 378–385.
9 C. S. Ribeiro, J. Z. Y. Tan, M. M. Maroto-Valer and M. A. Lansarin, *J. Environ. Chem. Eng.*, 2021, **9**, 105097–105106.
10 H. Wang, L. Zhang, K. Wang, X. Sun and W. Wang, *Appl. Catal., B*, 2019, **243**, 771–779.
11 L. Liu, H. Zhao, J. M. Andino and Y. Li, *ACS Catal.*, 2012, **2**, 1817–1828.
12 H. Zhong, M. Ghorbani-Asl, K. H. Ly, J. Zhang, J. Ge, M. Wang, Z. Liao, D. Makarov, E. Zschech, E. Brunner, I. M. Weidinger, J. Zhang, A. v. Krasheninnikov, S. Kaskel, R. Dong and X. Feng, *Nat. Commun.*, 2020, **11**, 1409–1418.
13 P. Huang, J. Huang, S. A. Pantovich, A. D. Carl, T. G. Fenton, C. A. Caputo, R. L. Grimm, A. I. Frenkel and G. Li, *J. Am. Chem. Soc.*, 2018, **140**, 16042–16047.
14 R. Zhou and M. I. Guzman, *J. Phys. Chem. C*, 2014, **118**, 11649–11656.
15 B. Chon, S. Choi, Y. Seo, H. S. Lee, C. H. Kim, H. J. Son and S. O. Kang, *ACS Sustainable Chem. Eng.*, 2022, **10**, 6033–6044.
16 C. Dette, M. A. Pérez-Osorio, C. S. Kley, P. Punke, C. E. Patrick, P. Jacobson, F. Giustino, S. J. Jung and K. Kern, *Nano Lett.*, 2014, **14**, 6533–6538.
17 R. S. Vemuri, M. H. Engelhard and C. v. Ramana, *ACS Appl. Mater. Interfaces*, 2012, **4**, 1371–1377.
18 M. Pawar, S. T. Sendoğdular and P. Gouma, *J. Nanomater.*, 2018, **2018**, 5953609–5953621.
19 G. Rainò, M. A. Becker, M. I. Bodnarchuk, R. F. Mahrt, M. v. Kovalenko and T. Stöferle, *Nature*, 2018, **563**, 671–675.
20 A. Inbal, J. P. Ampuero and R. W. Clayton, *Science*, 2016, **354**, 88–92.
21 Y. F. Xu, X. D. Wang, J. F. Liao, B. X. Chen, H. Y. Chen and D. B. Kuang, *Adv. Mater. Interfaces*, 2018, **5**, 1801015–1801022.
22 F. Xu, K. Meng, B. Cheng, S. Wang, J. Xu and J. Yu, *Nat. Commun.*, 2020, **11**, 4613–4621.
23 J. S. Martin, N. Dang, E. Raulerson, M. C. Beard, J. Hartenberger and Y. Yan, *Angew. Chem., Int. Ed.*, 2022, **61**, e202205572–e202205579.
24 X. Liu, H. Zhao, L. Wei, X. Ren, X. Zhang, F. Li, P. Zeng and M. Liu, *Nanophotonics*, 2021, **10**, 1967–1975.
25 H. Algadi, C. Mahata, J. Woo, M. Lee, M. Kim and T. Lee, *Electronics*, 2019, **8**, 678–690.
26 J. Fujisawa, T. Eda and M. Hanaya, *Chem. Phys. Lett.*, 2017, **685**, 23–26.
27 S. A. Kumar, J. S. Shankar and B. K. Periyasamy, *J. Mater. Sci.*, 2022, **57**, 12449–12462.

 This journal is © The Royal Society of Chemistry 2023